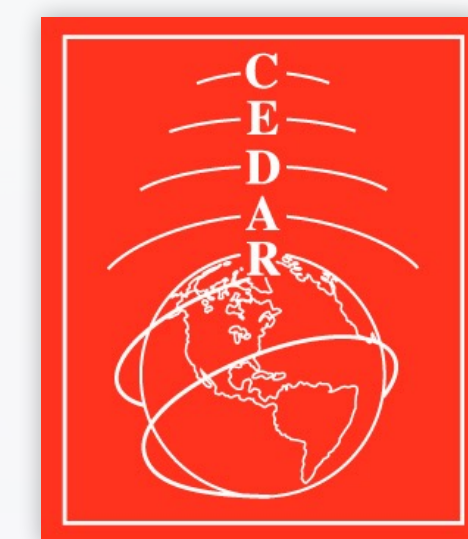


# Observability and detectability challenges in ground- and space-borne airglow imaging of acoustic and gravity waves due to line-of-sight effects

Jaime Aguilar and Jonathan B. Snively | Embry-Riddle Aeronautical University, Daytona Beach, FL

Poster #: MLTG-01  
CEDAR Workshop 2018  
Santa Fe, NM



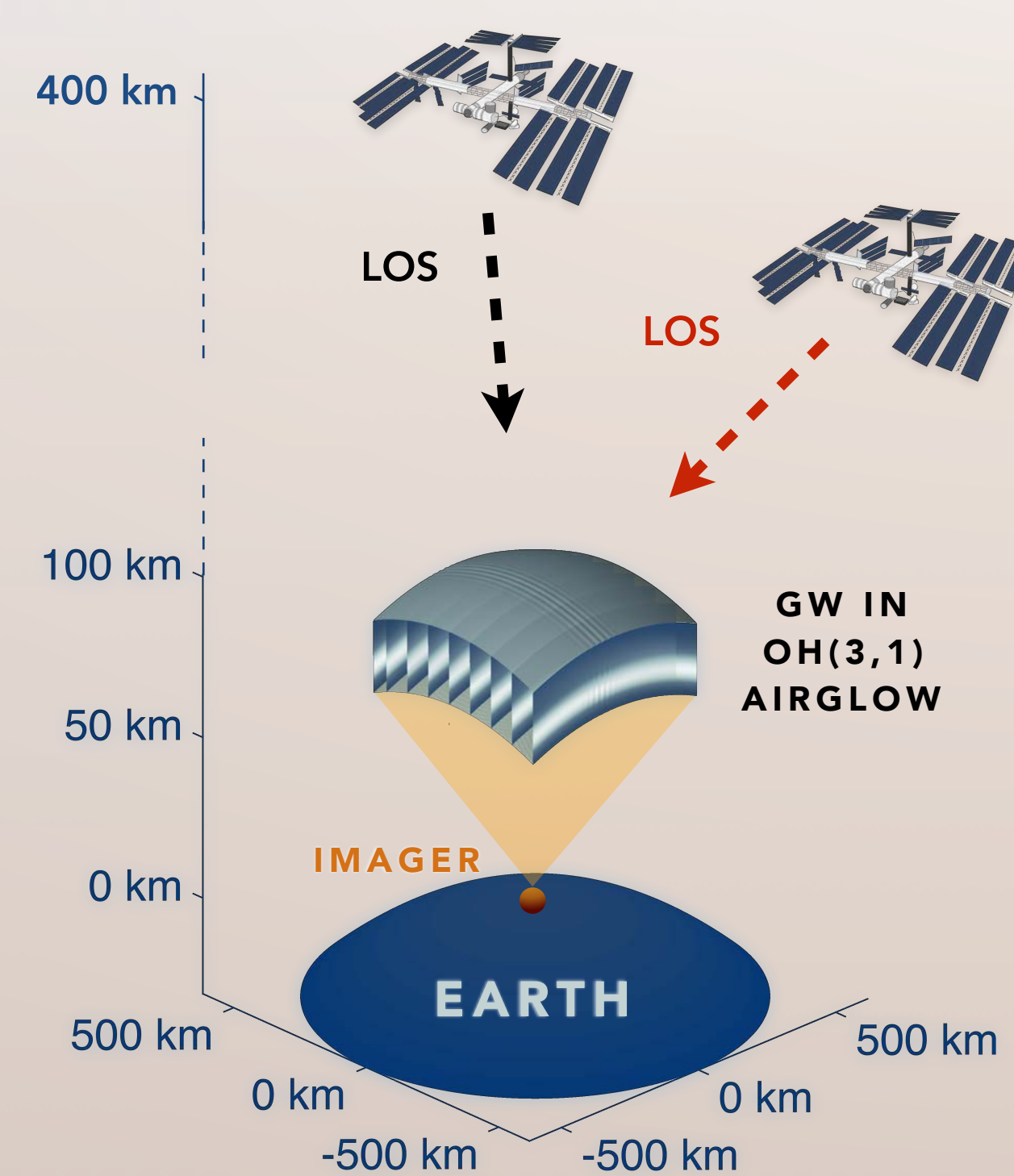
CEDAR  
Wiki link:



## Off-zenith imaging

### The all-sky imager & ground-based Observations

All-sky airglow imager data provides the clearest insight into wave processes centered near angles closer to zenith ( $\pm 45$  deg). The location is fixed and the spatial resolution decreases at larger angles from zenith across the FOV

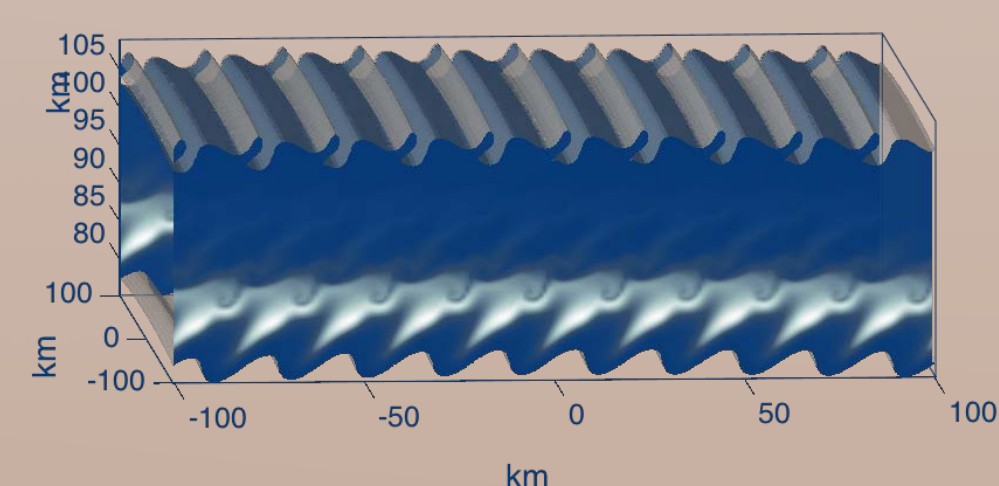


### Space-borne observations

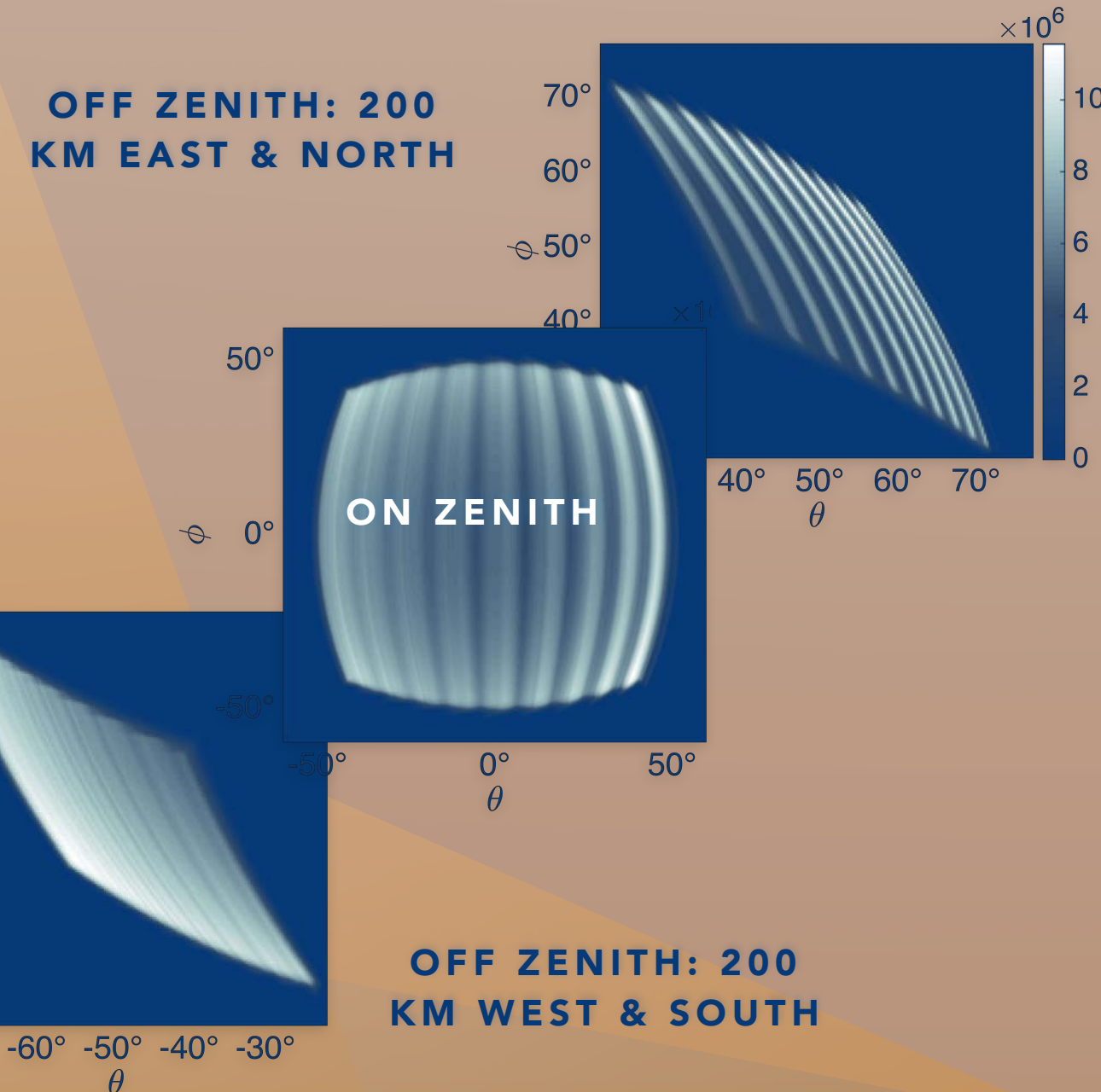
Imagers onboard moving platforms may capture different LOS across the airglow layer (viewing wave features from different angles as they pass) that can be chosen to better image features that are sensitive to LOS effects.

### Off-zenith imaging

Airglow observations made at steep viewing angles lead to scale filtering effects. The integration (imaging) of the vertical emission rates represents loss of information regarding the structure of the airglow layer as it effectively "flattens" it. While this process is non-invertible for real imager data, the use of simulated airglow structures enables direct comparisons to the structures present within the emitting layers.



Top: Example of a breaking GW, using the model of Snively et. al (2010), that is imaged at zenith and off zenith. Bottom left: oblique LOS leads to filtering. Bottom center: imaging over the zenith provides the most straightforward depiction of the wave. Bottom right: parallel LOS (aligned with the wavefronts) produces clear enhancements.

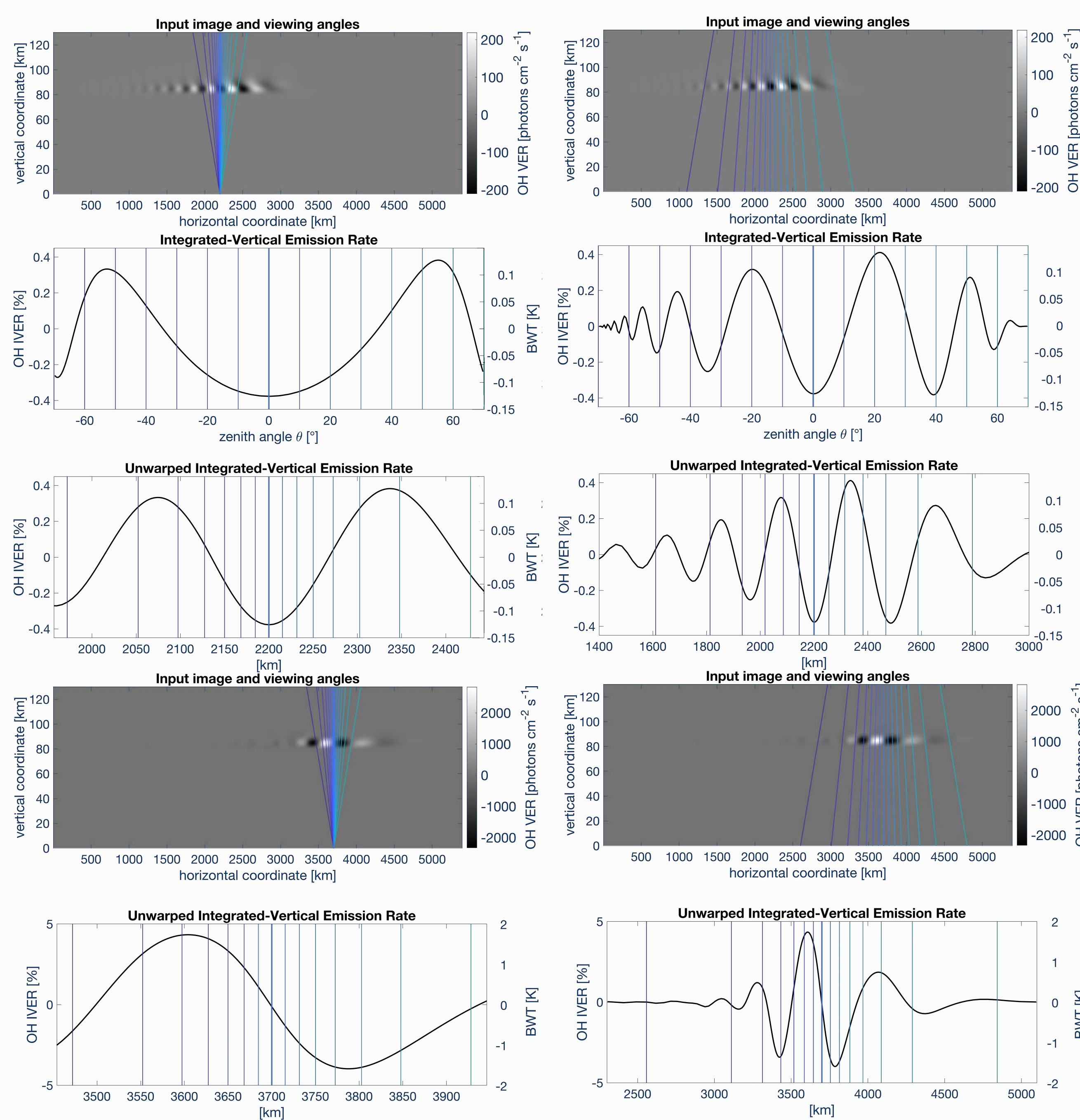


## Background and motivation: detectability challenges

Acoustic waves (AWs) have been predicted to be detectable by imaging systems for the OH airglow layer [Snively, GRL, 2013], and have been identified in spectrometer data [Pilger et al., JASP, 2013]. AWs are weak in the mesopause region, but can attain large amplitudes in the F region [Garcia et al., GRL, 2013] and have local impacts on the thermosphere and ionosphere. Similarly, fast GWs, with phase speeds over 100 m/s, may propagate to the thermosphere and impart significant local body forcing [Vadas and Fritts, JASTP, 2004]. Both have been clearly identified in ionospheric total electron content (TEC), such as following the 2013 Moore, OK, EF5 tornado [Nishioka et al., GRL, 2013] and following the 2011 Tohoku-Oki tsunami [e.g., Galvan et al., 2012; Zettergren et al., JGR, 2017], but AWs have yet to be unambiguously imaged in MLT data and fast GWs have low amplitudes near the threshold of detection. The associated detectability challenges are related to the transient nature of their signatures and to systematic challenges due to line-of-sight (LOS) effects such as enhancements and cancelations due to integration along aligned or oblique wavefronts and geometric intensity enhancements. It has been suggested these LOS effects introduce biases to the measured GW parameters for upward propagating waves [Hines and Tarasick, PSS, 1987; Hickey et al., JGR, 2010]. However, these biases may provide enough intensity enhancements to allow for the detection of certain phenomena in the OH airglow measurements that otherwise would be beneath the sensibility threshold of imaging instruments.

## Simulating an airglow-imager environment

We employ a synthetic "airglow imager" framework that incorporates 2D and 3D modeled emission rate data and performs the necessary LOS integrations to generate synthetic data from ground-based or satellite platforms. We model acoustic and gravity wave perturbations to the OH(3,1) emission using a nonlinear, compressible model [e.g., Snively et al., JGR, 2010] to construct controlled AW and GW as generated by surface forcing from below. Sources are based on the 2011 Tohoku-Oki tsunami ocean surface transient and simulations reported by [Zettergren et al., JGR, 2017], and the tsunami source definitions by Hickey et al. [2009] and Laughman et al. [2017].



## Concluding remarks

The synthetic airglow imager framework allows us to diagnose the observability challenges associated with large-scale GWs and understand the effects of imaging obliquely through dense layers. First is the case of ground-based imagers observing these phenomena; sea-borne platforms for imaging of tsunamigenic GWs are not practical to implement and have narrow domains at the airglow height that limit the observation capabilities. Still, we suggest that keograms from these ground-based imagers can provide basic GW parameters just as well as those observed by satellite imagers. In the case of these space-borne imagers, the observed larger domains feature significant LOS effects, one of those being the appearance of a slight curvature of the IVER suggesting a *phase change due purely to LOS effects* (oblique imaging of the large-scale wavefronts) on top of the wave phase progression. We also analyzed the intensity enhancements that occur at large FOVs using the acoustic wave generated by the source of the same tsunami. These results suggest that detectability challenges associated with small amplitudes can be mitigated by observing off-zenith at very large FOVs, or by pointing the imager at those directions (viewing over sources). This framework allows us to investigate specific cases and pinpoint the preferred viewing geometries for each studied phenomena in hopes to learn how to better leverage real airglow imager data.

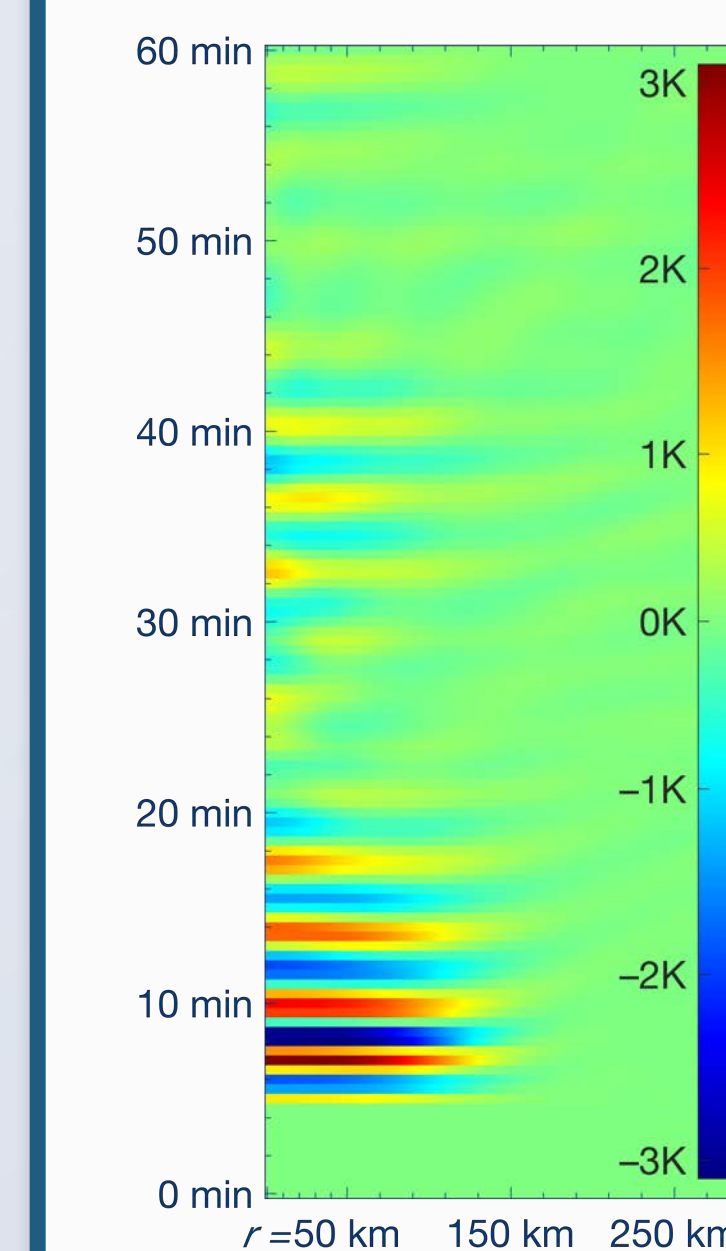
Acknowledgements: This research was supported under NSF grant 1151746.

Contact: Jaime Aguilar, aguila9@my.erau.edu, Department of Physical Sciences, Embry-Riddle Aeronautical University, Daytona Beach FL 32114

$$*BWT(x,t) = \frac{\int \epsilon(x,z,t)T(x,z,t) dz}{\int \epsilon(x,z,t) dz}$$

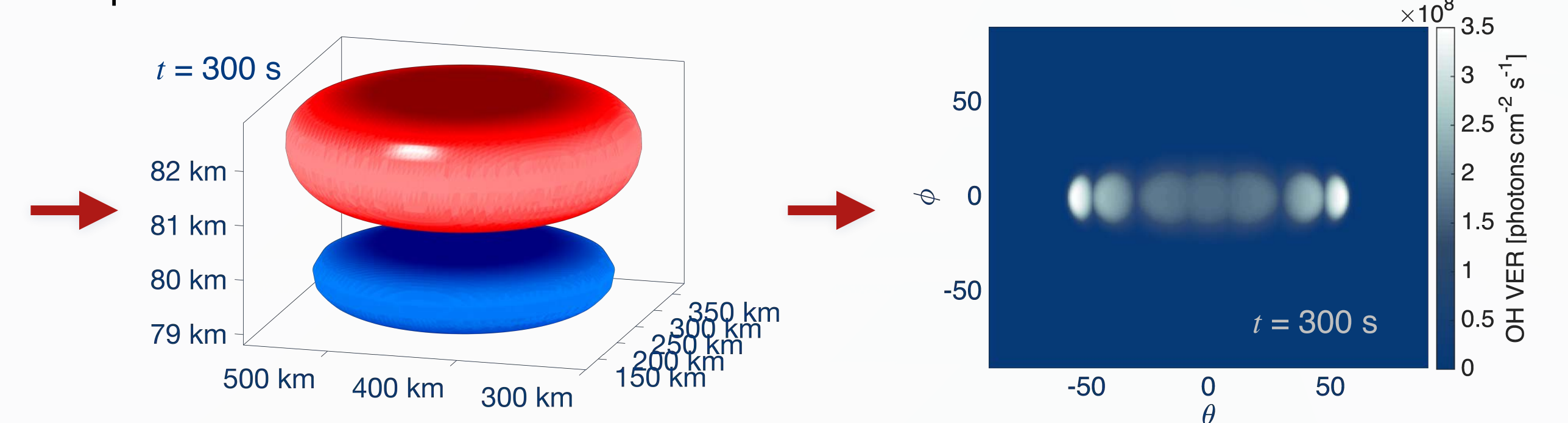
\*BWT - brightness-weighted temperature,  $\epsilon$  - volume emission rate,  $T$  - temperature

EMBRY-RIDDLE  
Aeronautical University



## Imaging tsunami-induced acoustic waves

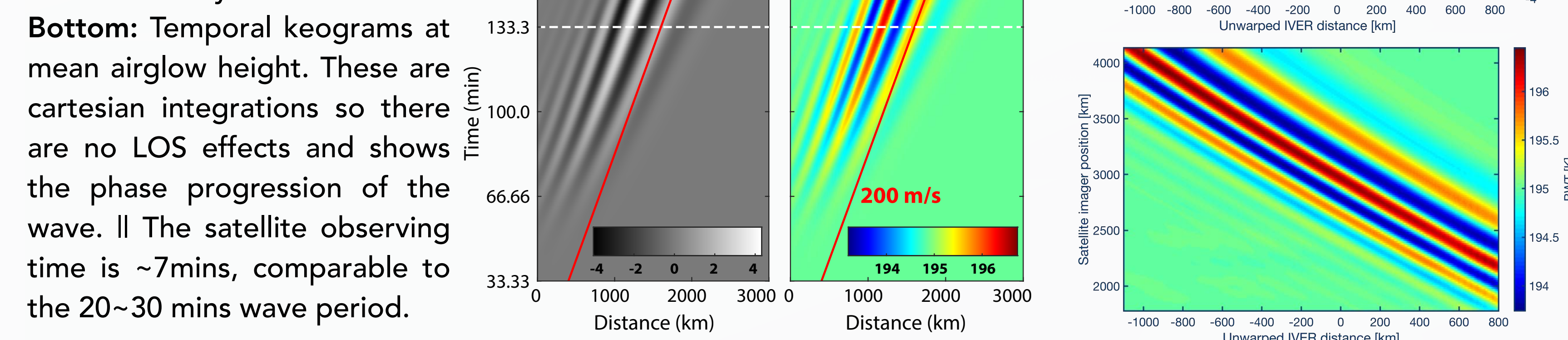
The 2011 Tohoku-Oki earthquake ocean surface disturbance that subsequently led to the tsunami has been approximated and used as the acoustic wave source for this study. The modeled data spans an hour of the dynamical evolution of the perturbations after the surface disturbance. However, in this study we use the 3D output at  $t = 300$  s.



Left: Temporal evolution of the acoustic temperature signal in [K] at fixed height of 85 km. Center: 3D isosurface spatial visualization at  $t = 300$ s. Right: Intensity synthetic CCD images as seen from a space-borne imager at 400 km altitude and orbital positions: -500 km, -300 km, -100 km, nadir, 100 km, 300 km and 500 km from AW source, all at  $t = 300$ s.

## Imaging geometries for a tsunamigenic large-scale gravity wave.

Left: LOS integrations of a ground- and a satellite-based imager (~400 km height) at two different times, top at 4,000s and bottom at 10,000s from the onset of the GW simulation of the OH(3,1) airglow response due to the tsunami. The results are presented as perturbations to the background mean. Notice the order of magnitude difference in the signatures between both times. The signature at 4000s is approaching observability, while at 10,000s it is likely observable by contemporary imagers. The phase of the Krassovsky ratio is close to zero, so the BWT plots are phased-aligned with the IVER plots. Due to the larger coverage of the satellite imager FOV at the airglow height, more wavelengths are observed and available for analysis. Right: Spatial "keograms" representing a moving imager and their respective IVERs observing a *time-fixed* wave; since there is no phase progression, the curvature seen in the keogram represents a phase change attributed only to LOS effects.



Bottom: Temporal keograms at mean airglow height. These are cartesian integrations so there are no LOS effects and shows the phase progression of the wave. The satellite observing time is ~7mins, comparable to the 20~30 mins wave period.